Proceedings of ERAD (2002): 73–77 © Copernicus GmbH 2002

ERAD 2002

Polarimetric data evaluation in severe storms using two research dual-polarized radars

V. N. Bringi, Y. Wang, and J. Hubbert

Dept. of Electrical & Computer Engineering, Colorado State University, Fort Collins, CO 80523, USA

Abstract. A procedure is developed for evaluating antenna-induced polarimetric errors in the presence of large spatial gradients of precipitation echo. Synthetic storm simulations are used to develop a methodology for masking error regions in the Z_{dr}, L_{dr} and K_{dp} fields. Data in a severe storm from the CSU-CHILL and NCAR-SPOL radars, both of which operate at S-band, are used to illustrate the methodology.

1 Introduction

The theoretical basis of polarimetric radar meteorology is the close connection between the scattering matrices of precipitation targets and their physical characteristics. The polarimetric radar employs the covariance matrix to retrieve the relative information for the random medium case. With two orthogonal polarization transmission and dual-channel receiver, the full covariance matrix and relative radar signatures can be reconstructed.

However, it is impossible to build a radar system with pure orthogonal polarization transmission and a dual-channel receiver with perfect isolation. The reconstruction will be complicated due to system polarization errors (McCormick 1981; Metcalf and Ussailis, 1984). In practice, the cross polarization contamination of the co-polar channel signals can be ignored. However, in cross-polar channel, the weak power from targets may come in at the same level as the leaked power from the co-polar channel.

Since the precipitation is distributed in space, large spatial gradients of the precipitation echo across the radar beam can cause error. Once the medium is not homogenous, the gradient should be evaluated as well in order to make reliable applications of the polarimetric radar data. Therefore, it is necessary to check the whole antenna pattern and the actual gradients in 3-D space. The Severe Thunderstorm Electrification and Precipitation Study (STEPS) deployed two research dual-polarization radars, CSU-CHILL and NCAR-SPOL, at different locations, so the comparison between the two radars provides a possibility to evaluate the polarimetric data under large gradient scenario.

Correspondence to: V. N. Bringi
(bringi@engr.colostate.edu)

2 Theoretical model of polarization errors

Following the convention in Bringi and Chandrasekar (2001), we denote the 'intrinsic' scattering matrix as

$$\mathbf{S} = \begin{bmatrix} S_{hh} & S_{hv} \\ S_{vh} & S_{vv} \end{bmatrix} \tag{1}$$

and the measured scattering matrix as

$$\mathbf{V} = \begin{bmatrix} V_{hh} & V_{hv} \\ V_{vh} & V_{vv} \end{bmatrix} \tag{2}$$

where the first element in the subscript refers to receiving polarization while the second refers to transmitting polarization. The cross polarization contamination and the gain inequality between two channels can be expressed by an error matrix (McCormick 1981). In this paper, we combine the error matrix into the antenna gain,

$$\mathbf{G} = \begin{bmatrix} g_h & e_v \\ e_h & g_v \end{bmatrix} \tag{3}$$

Under alternate H, V polarization scheme, the measured scattering matrix follows,

$$\mathbf{V}(\theta,\phi) = \int\int \mathbf{G}_{rx}(\theta'-\theta,\phi'-\phi) \mathbf{S}(\theta',\phi')\mathbf{G}_{tx}(\theta'-\theta,\phi'-\phi)d\Omega' \tag{4}$$

where 'rx' describes receiving channel and 'tx' describes transmission channel. The integration over solid angle takes effect on spherical surfaces that are centered on the radar location. We can drop the integration off at the intermediate steps to simplify the derivation so that,

$$\mathbf{V} = \mathbf{G}_{rx}\mathbf{S}\mathbf{G}_{tx} \tag{5}$$

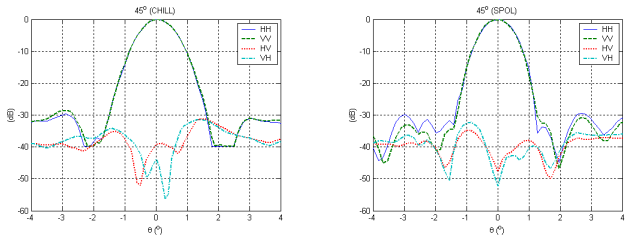

Fig. 1. On-axis cuts of the CSU-CHILL and NCAR-SPOL antenna patterns on 45° plane

Equation (5) indicates that the measured scattering matrix relates to the intrinsic scattering matrix through a group of independent linear equations. To simplify (5) further, we need several relations and approximations:

a. Reciprocity of the polarimetric radars, which implies $\mathbf{G}_{rx} = \mathbf{G}_{tx}^T$;

b. Reciprocity of the scattering medium, which implies $S_{hv} = S_{vh}$;

c. Well-designed antennas, which implies $g_h \gg e_h$ and $g_v \gg e_v$;

d. "Mirror" reflection symmetry about zero mean canting angle, which implies $< S_{hh}S_{vh}^* >=< S_{vv}S_{vh}^* >= 0$.

We approximate the co-polar measurements to the first order of polarization errors, and the cross-polar measurements to the second order of polarization errors. A sub-set of the relevant covariance matrix elements can be expressed as,

$$< |V_{hh}|^2 >= |g_h|^4 < |S_{hh}|^2 > \tag{6a}$$

$$< |V_{vv}|^2 >= |g_v|^4 < |S_{vv}|^2 > \tag{6b}$$

$$\begin{aligned} < |V_{vh}|^2 >= |g_h e_v|^2 < |S_{hh}|^2 > + |g_v e_h|^2 < |S_{vv}|^2 > \\ +2Re\Big[g_h g_v^* e_h^* e_v < S_{hh}S_{vv}^* > \Big] \\ +\Big\{|g_h g_v|^2 + 2Re[g_h g_v e_h^* e_v^*]\Big\} < |S_{vh}|^2 > \end{aligned} \tag{6c}$$

$$< V_{hh}V_{vv}^* >= g_h^2 g_v^{*2} < S_{hh}S_{vv}^* > \tag{6d}$$

Notice that the convolution in (4) is implicit in the above equations.

To first order, Z_{dr} can be expressed as,

$$Z_{dr} = \frac{\int\int |g_h|^4 < |S_{hh}|^2 > d\Omega'}{\int\int |g_v|^4 < |S_{vv}|^2 > d\Omega'} \tag{7}$$

which gets biased and the error direction is unpredictable because of convolution in both denominator and numerator, as indicated by (7). Usually the co-polar patterns of the main lobe are well matched except for a constant gain inequality between the H and V-ports, but this is not the case for the sidelobes (see the antenna patterns in Fig. 1). Therefore,

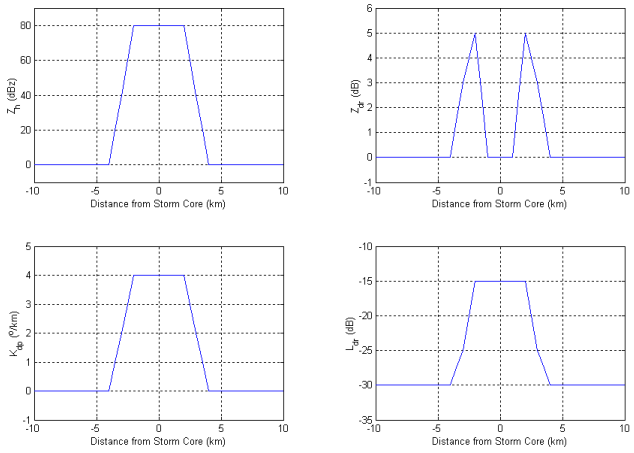

Fig. 2. Intrinsic profiles of Z_h, Z_{dr}, K_{dp} and L_{dr} for the synthetic storm.

once the sidelobes fall into high reflectivity regions, the Z_{dr} polarization error may go up to a noticeable level and such sidelobe mismatch will complicate the analysis (Pointin et al., 1988).

Measured L_{dr} can be lager than the intrinsic value due to the leakage of co-polar power in the cross-polar channel. From (6c), it is clear that co-polar terms affect the measurement through the cross-polar antenna pattern. The approximate bias in L_{dr} due to polarization error can be expressed as,

$$\begin{aligned} \Delta L_{dr} = \Bigg\{ \int\int |g_h e_v|^2 < |S_{hh}|^2 > \\ d\Omega' + \int\int |g_v e_h|^2 < |S_{vv}|^2 > d\Omega' \\ +2Re \int\int g_h g_v^* e_h^* e_v < S_{hh}S_{vv}^* > d\Omega' \Bigg\} \\ / \Bigg\{ \int\int |g_h|^4 < |S_{hh}|^2 > d\Omega' \Bigg\} \end{aligned} \tag{8}$$

Similar to Z_{dr}, if the intrinsic Φ_{dp} fluctuates sharply across the radar beam, or uniform distributed phase error exists in the sidelobes of the antenna pattern, then ρ_{co} as shown in (9) will be probably measured with a lower value in low reflectivity area due to the cancellation among different phasors. Since Φ_{dp} is the argument of ρ_{co}, K_{dp} may get positive or negative biases as well.

$$\rho_{co} = \frac{\int\int g_h^2 g_v^{*2} < S_{hh}S_{vv}^* > e^{-j\Phi_{dp}} d\Omega'}{\sqrt{\int\int |g_h|^4 < |S_{hh}|^2 > d\Omega' \cdot \int\int |g_h|^4 < |S_{hh}|^2 > d\Omega'}} \tag{9}$$

3 Simulations and methodology

Although the polarization errors analyzed in the previous section result from the convolution between the antenna pattern and the non-uniform reflectivity, the gradient in precipi-

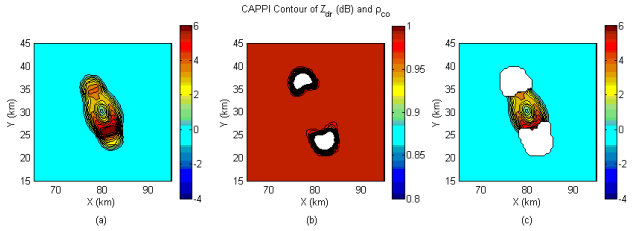

Fig. 3. CAPPI plots of Z_{dr} and ρ_{co} on the 5 km elevation plane for the synthetic storm: **(a)** 'measured' Z_{dr}, which is contaminated with errors; **(b)** simulated ρ_{co} after convolution (values less than 0.8 are not shown); **(c)** 'masked' Z_{dr} with errors indicated in white.

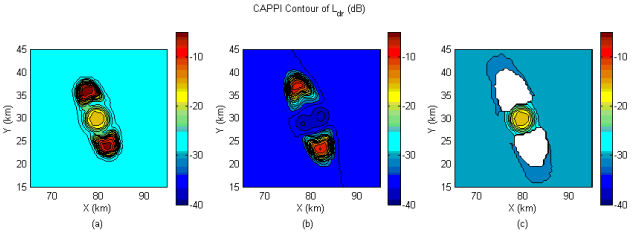

Fig. 4. CAPPI plots of L_{dr} on the 5 km elevation plane: **(a)** 'measured' L_{dr}; **(b)** estimated L_{dr} bias; **(c)** 'masked' L_{dr} after bias adjustment.

tation echo cannot by itself be used to locate the region contaminated by errors.

To implement the convolution, the intrinsic values of S_{hh}, S_{vv} and S_{vh} should be known first, which seems impossible, besides the 2-D antenna pattern. However, from (6), the dominant errors come from gradients in S_{hh} and S_{vv} when the intrinsic L_{dr} is small (and we are interested in the errors when the intrinsic L_{dr} is small). From (6a) and (6b), it is indicated that the measurements of V_{hh} and V_{vv} are not much affected. Therefore, it is reasonable to assume the measured reflectivity is approximately equal to the intrinsic value.

To illustrate the polarization errors induced by the antenna pattern, we simulated a synthetic storm cell with simple spherical symmetric structure. The 3-D synthetic storm is assumed with its core 'located' at 80 km east and 30 km north of the CSU-CHILL radar and 5 km in elevation. One cut through the synthetic storm core is shown in Fig. 2.

First we interpolate the 4 available patterns (at 0°, 45°, 90° and 135° planes) of the CSU-CHILL antenna so as to construct the full 2-D pattern. The NCAR-SPOL 2-D pattern comes directly from far-field test measurements. In addition, we have introduced random phase beyond the main lobe of the antenna co-polar pattern. Then for every fixed range, we implement 2-D convolution along the spherical surface as given by (6). The radar 'measurements' are obtained by the first convolution with the synthetic storm. And then assuming these 'measured' radar signatures as intrinsic values, we obtain estimations about ρ_{co}, L_{dr} bias and K_{dp} with another convolution.

We assume the intrinsic ρ_{co} to be 1 in order to get rid of

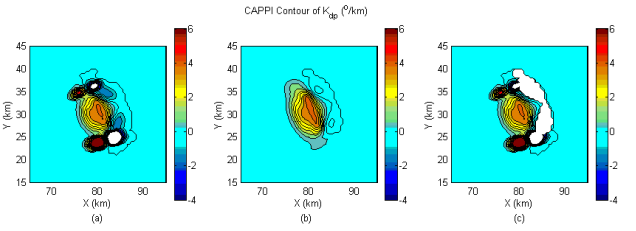

Fig. 5. CAPPI plots of K_{dp} on the 5 km elevation plane: **(a)** 'measured' K_{dp}; **(b)** estimated K_{dp} assuming that the input Φ_{dp} from **(a)** is monotone increasing with range; **(c)** 'masked' K_{dp}.

the effect of physical precipitation randomness. In the simulation, we reconstruct ρ_{co} following the convolution based on (9). The decrease of such simulated ρ_{co} can be used as an indicator of Z_{dr} error. If simulated ρ_{co} is less than 0.99, we mask the Z_{dr} value as 'bad' in such location. Figure 3 shows CAPPI plot of the 'measured' Z_{dr}, the simulated ρ_{co}, and 'masked' Z_{dr} on the 5 km elevation plane. The error regions get detected dramatically even thought some residues still exist (see white 'masked' region in Fig. 3). For confident rain rate estimation, Z_{dr} bias should be confined within 0.2 dB while 0.5 dB is acceptable for hydrometeor classification. Usually, the antenna performance can meet or exceed such constraint if the medium is homogenous. However, once large gradient exists in target volume as shown in this simulation, the Z_{dr} bias will be much larger and may be out of 0.5 dB range.

For L_{dr}, our objective is aimed at estimating the system bias as indicated by (8). It is difficult to obtain the accurate complex error terms, e_h and e_v, so we drop off the phase terms and use $|g_h g_v e_h e_v|$ directly (which makes the bias estimation a little larger). In addition, taking the propagation effect into account, the co-polar covariance is equivalent to

$$< S_{hh} S_{vv}^{*} >= |S_{hh} S_{vv}| e^{-j\Phi_{dp}} \tag{10}$$

The convolution based on (8) gives the L_{dr} bias directly and this estimate is used to adjust the 'measured' L_{dr}. If the bias exceeds -32 dB for CHILL and -28 dB for SPOL, we mask the regions as 'bad' data. Figure 4 also shows the similar CAPPI plot (to Fig. 3). Nearly all the extreme L_{dr} errors are masked out, as indicated by the white 'masked' region in Fig. 4. L_{dr} is valuable in hydrometeor classification and its bias should be confined within 1 or 2 dB. Note that the effect of such bias depends on the intrinsic L_{dr} level, e.g. less effect when detecting highly depolarizing hailstones or wet snowflakes.

Figure 5a shows that in the 'measured' K_{dp} data, negative K_{dp} occurs even though the intrinsic K_{dp} is non-negative as indicated by Fig. 2. Usually, negative K_{dp} is only expected in the upper parts of a thunderstorm due to vertically oriented ice crystals, and very infrequently in hailstorms. Next, we force the 'measured' Φ_{dp} (from Fig. 5a) to be monotone increasing with range, and obtain, after convolution, Fig. 5b which is used as the basis for masking the K_{dp} error regions (as shown in Fig. 5c). That is, areas in Fig. 5b where

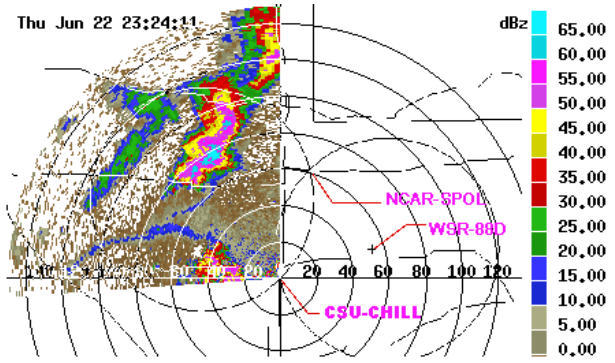

Fig. 6. PPI plot of the 22 June 2000 storm case showing the locations of the CSU-CHILL and NCAR-SPOL radars during the STEPS projects.

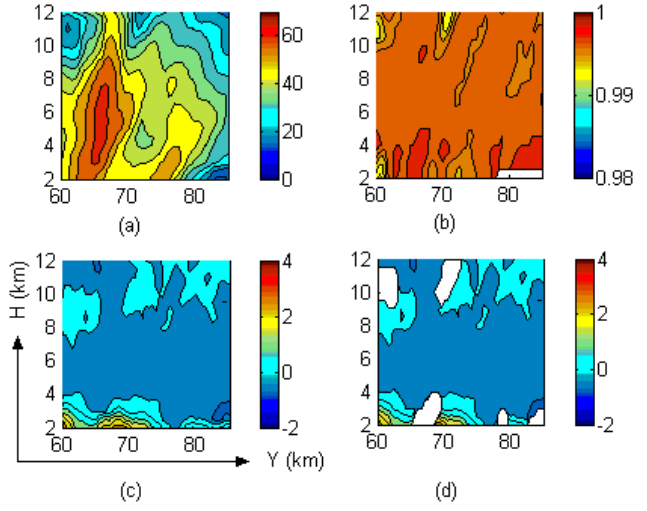

Fig. 7. Vertical section through the storm case of Fig. 6, **(a)** measured reflectivity Z_h, **(b)** simulated ρ_{co}; **(c)** measured Z_{dr} and **(d)** masked Z_{dr}, all from NCAR-SPOL.

$K_{dp} < 0$ are used as the basis for the mask shown in Fig. 5c. We acknowledge that not all of the errors could be masked and the positive K_{dp} error cannot be masked by this method, but it is helpful to sort out most of contaminated negative K_{dp} area. The K_{dp} bias (in deg/km) should meet similar criteria as stated for the Z_{dr} bias. This simulation shows that K_{dp} may be measured with large bias if large gradients of reflectivity and/or Φ_{dp} exist across the beam.

4 Evaluation of measurements during STEPS

The STEPS project was conducted in eastern Colorado during the summer of 2000. Figure 7 shows the storm event of 22 June, which was observed by the CSU-CHILL and NCAR-SPOL radars. This storm had large gradients in reflectivity and 2.5 cm hail was reported. Our goal is to mask out antenna-induced errors for both radar data sets. Our methodology is based on the synthetic storm simulations pre-

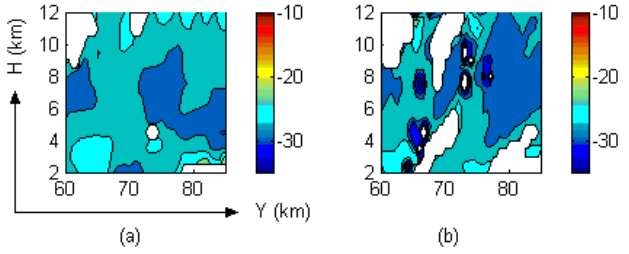

Fig. 8. Vertical section of masked L_{dr} after estimated system bias removed, **(a)** from CSU-CHILL and **(b)** from NCAR-SPOL.

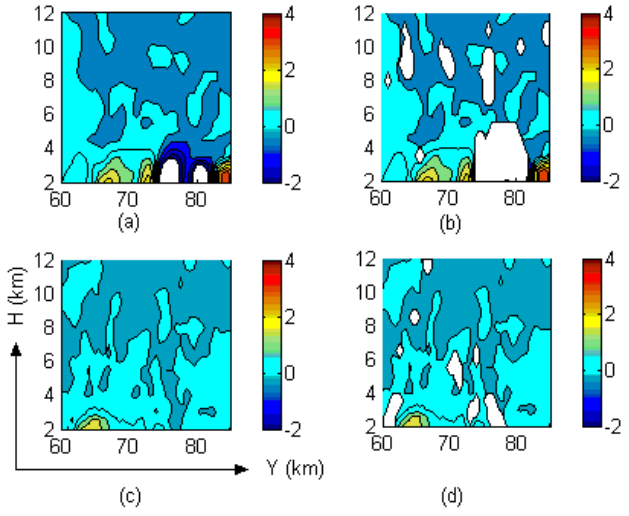

Fig. 9. Vertical section of **(a)** measured K_{dp} (values less than -2 are not shown) and, **(b)** masked K_{dp} from CSU-CHILL. Panel **(c)** and **(d)** are similar but for NCAR-SPOL.

sented in Sect. 3, i.e. the measured reflectivity is assumed as intrinsic value and 2-D convolution is implemented over spherical surfaces in the selected 3-D volume to estimate the error structure. The surface can be constructed from the data set with range fixed, but interpolation is necessary to account for non-uniform scan angles.

To mask out Z_{dr} errors, we first simulate ρ_{co} by convolving the measured reflectivity with the antenna pattern (which has random phase in the sidelobe region) assuming intrinsic ρ_{co} to be 1. This is similar to the procedure of getting Fig. 3b. The Z_{dr} mask is based on the simulated ρ_{co} falling below 0.995. For example, Fig. 7a shows the measured reflectivity from NCAR-SPOL radar (as a vertical section through the storm core), Fig. 7b shows the simulation of ρ_{co}, Fig. 7c shows the measured Z_{dr}, and Fig. 7d shows the masked Z_{dr}. Note the mask region near $Y = 68$ km (height = 3 km) which is near a region of low reflectivity imbedded within two regions of high reflectivity (see Fig. 7a).

The masked L_{dr} field is based on estimated ΔL_{dr} (see Eq. 8). Next, this bias is removed from the measured L_{dr}. The mask is based on regions where ΔL_{dr} is larger than -32 dB for the CSU-CHILL and -28.5 dB for NCAR-SPOL (these thresholds are based on a histogram analysis) and re-

flects the fact that the CSU-CHILL's L_{dr} system limit is lower than NCAR-SPOL's limit because of better antenna cross-polar performance. Figure 8a shows the masked L_{dr} from CSU-CHILL and Fig. 8b form NCAR-SPOL.

For K_{dp} mask, we force the measured Φ_{dp} to be monotone increasing with range, then perform the convolution and reconstruct K_{dp}. Regions where the re-constructed $K_{dp} < 0$ is used to mask the measured K_{dp} field. Figures 9a and b show the measured K_{dp} and masked K_{dp} for CSU-CHILL; similar results are shown in Figs. 9c and d for NCAR-SPOL.

Compared to the simulation illustrated in the previous section, the antenna-induced errors in this particular case don't seem too outstanding, such as the simulated ρ_{co} being only as low as around 0.99, and no much negative K_{dp} showing on the estimation. However, for supercell storms, the large gradients (exceeding 40 dB/km) can distort the measurement greatly such that hydrometeor classification may be in error. For more modest gradients (e.g., < 20 dB/km) such as found in rainstorms and depending on geometry, the antenna-induced errors in Z_{dr} and K_{dp} may be within acceptable limits for quantitative rain rate estimation for antennas of the quality of the CSU-CHILL or SPOL radar.

5 Conclusion

Our synthetic storm simulations show a possible procedure for detecting antenna-induced errors (in the presence of large gradients) in the polarimetric data. The full 2-D antenna patterns (co- and cross-polar) must be known, and we further introduce random phase outside the main lobe to more realistically simulate ρ_{co} and Φ_{dp} errors. We have used measured data from a severe, convective storm with large spatial gradients to illustrate the detection of antenna-induced errors in Z_{dr}, L_{dr}, and K_{dp}. Such masking will be useful for improving data quality without 'correcting' the data, especially when such data are used for rain rate estimation and hydrometeor classification. Procedures for 'correcting' the polarimetric data when the precipitation is homogenous can be found in McCormick (1981), Metcalf and Ussailis (1984) or Moisseev et al. (2001). However, considering the antenna-induced errors, correction is infeasible since even the estimation of error structure is very complicated as shown in this work. To improve the data quality for such scenario, we must use well-designed antennas with excellent sidelobe performance, e.g. as afforded by single offset or dual-offset antenna designs. We are in the process of acquiring a new 9 m dual-offset Gregorian antenna for the CSU-CHILL radar.

Acknowledgement. This research was supported by the National Science Foundation via grant ATM-9982030.

References

Bringi, V.N., and V. Chandrasekar, 2001: Polarimetric Doppler Weather Radar. Cambridge University Press.

McCormick, G.C., 1981: Polarization errors in a two-channel system, Radio Sci., Vol.16, pp. 67-75.

Metcalf, J.I., and J.S. Ussailis, 1984: Radar System Errors in Polarization Diversity Measurements, J. Atmos. Oceanic Technol., Vol. 1, pp. 105-114.

Moisseev, D.N., C.M.H. Unal, H.W.J. Russchenberg, and C.P. Ligthart, 2001: Improvement of Polarimetric Radar Calibration for Atmospheric Radars, 30th International Conference on Radar Meteorology, pp.26-28.

Pointin, Y, D. Ramond, and J. Fournet-Fayard, 1988: Radar Differential Reflectivity Z_{dr}: A Real-Case Evaluation of Errors Induced by Antenna Characteristics, J. Atmos. Oceanic Technol., Vol. 5, pp. 416-423.